ADVANCES IN ATMOSPHERIC SCIENCES, VOL. 29, NO. 4, 2012, 647–660

Modulation of El Niño-Southern Oscillation by Freshwater Flux and Salinity Variability in the Tropical Pacific

ZHANG Rong-Hua*[1] (张荣华), ZHENG Fei[1,2] (郑 飞), ZHU Jieshun[3] (朱杰顺), PEI Yuhua[1,4,5] (裴玉华), ZHENG Quanan[6] (郑全安), and WANG Zhanggui[7] (王彰贵)

[1]*Earth System Science Interdisciplinary Center, University of Maryland, College Park, Maryland, USA*

[2]*International Center for Climate and Environment Science, Institute of Atmospheric Physics, Chinese Academy of Sciences, Beijing* 100029

[3]*Center for Ocean-Land-Atmosphere Studies, Institute of Global Environment and Society, Calverton, Maryland, USA*

[4]*The College of Physical and Environmental Oceanography, Ocean University of China, Qingdao* 266003

[5]*State Key Laboratory of Satellite Ocean Environment Dynamics, Second Institute of Oceanography, State Oceanic Administration, Hangzhou* 310012

[6]*Department of Atmosphere and Ocean Science, University of Maryland, College Park, Maryland, USA*

[7]*National Marine Environmental Forecasting Center, State Oceanic Administration, Beijing* 100081

(Received 12 November 2011; revised 1 January 2012)

ABSTRACT

The El Niño-Southern Oscillation (ENSO) is modulated by many factors; most previous studies have emphasized the roles of wind stress and heat flux in the tropical Pacific. Freshwater flux (FWF) is another environmental forcing to the ocean; its effect and the related ocean salinity variability in the ENSO region have been of increased interest recently. Currently, accurate quantifications of the FWF roles in the climate remain challenging; the related observations and coupled ocean-atmosphere modeling involve large elements of uncertainty. In this study, we utilized satellite-based data to represent FWF-induced feedback in the tropical Pacific climate system; we then incorporated these data into a hybrid coupled ocean-atmosphere model (HCM) to quantify its effects on ENSO. A new mechanism was revealed by which interannual FWF forcing modulates ENSO in a significant way. As a direct forcing, FWF exerts a significant influence on the ocean through sea surface salinity (SSS) and buoyancy flux ($Q_{\rm B}$) in the western-central tropical Pacific. The SSS perturbations directly induced by ENSO-related interannual FWF variability affect the stability and mixing in the upper ocean. At the same time, the ENSO-induced FWF has a compensating effect on heat flux, acting to reduce interannual $Q_{\rm B}$ variability during ENSO cycles. These FWF-induced processes in the ocean tend to modulate the vertical mixing and entrainment in the upper ocean, enhancing cooling during La Niña and enhancing warming during El Niño, respectively. The interannual FWF forcing-induced positive feedback acts to enhance ENSO amplitude and lengthen its time scales in the tropical Pacific coupled climate system.

Key words: freshwater flux (FWF) forcing and feedback, sea surface salinity (SSS) variability, ENSO modulation, coupled ocean-atmosphere models

Citation: Zhang, R.-H., F. Zheng, J. S. Zhu, Y. H. Pei, Q. Zheng, and Z. G. Wang, 2012: Modulation of El Niño-Southern Oscillation by freshwater flux and salinity variability in the tropical Pacific. *Adv. Atmos. Sci.*, **29**(4), 647–660, doi: 10.1007/s00376-012-1235-4.

1. Introduction

El Niño-Southern Oscillation (ENSO) is a natural phenomenon centered in the tropical Pacific that significantly impacts climate variability and predictability worldwide. Numerous previous studies have identified roles of various forcings and feedbacks in ENSO processes. For example, Bjerknes (1969) first identified a feedback loop associated with ENSO, involving interactions among the winds, the thermocline,

*Corresponding author: ZHANG Rong-Hua, rzhang@essic.umd.edu

and sea surface temperature (SST) within the tropical Pacific (i.e., the Bjerknes feedback). Many other feedback processes have also been illustrated that can contribute to modulations of ENSO, including ocean biology-induced feedback (e.g., Timmermann and Jin, 2002; Zhang et al., 2009), tropical instability wave (TIW)-induced feedback (e.g., Zhang and Busalacchi, 2008), and so on. It has been well established that surface winds are a dominant driving force to ENSO cycles in the tropical Pacific, whereas surface heat flux acts as a negative feedback to the coupled system.

Another important atmospheric forcing to the ocean is freshwater flux (FWF), which directly affects sea surface salinity (SSS), a key variable in the interactions among the Earth's water cycle, ocean circulation, and climate (e.g., Lagerloef, 2002; US CLIVAR Salinity Working Group, 2007). Also, the FWF affects the depth of the mixed layer (MLD) through its direct contributions to buoyancy flux (Q_{B}), which further affects the entrainment of subsurface water into the mixed layer. Through these oceanic processes, FWF can have a significant role in climate variability in the tropical Pacific. Recently, various studies have shown that FWF forcing and its related salinity variability in the region are important to the tropical climate dynamics, including data analyses (e.g., Maes et al., 2002; Delcroix et al., 2007), ocean-only modeling experiments (e.g., Murtugudde and Busalacchi, 1998; Yang et al., 1999; Fedorov et al., 2004; Huang and Mehta, 2010), and coupled ocean-atmosphere modeling experiments (e.g., Zhang and Busalacchi, 2009; Hackert et al., 2011; Yu et al., 2011).

ENSO has been observed to exhibit significant modulations in its properties, including its amplitude and time scales (e.g., Zhang et al., 2008; Collins et al., 2010; Zhu et al., 2011). Although remarkable progress has been made in ENSO studies over the past several decades, the mechanisms for the modulations of ENSO are still not completely understood. In the past, great emphases have been placed on the roles of wind and heat flux (e.g., Zhu et al., 2007), but much less on those of FWF forcing and salinity effect. For example, various coupled ocean–atmosphere models have been developed for use in ENSO-related modeling studies, including intermediate coupled models (ICMs), hybrid coupled models (HCMs), and coupled general circulation models (CGCMs). However, FWF forcing has not been adequately represented in many state-of-the-art coupled models. In particular, FWF has not been even included in most ICMs and HCMs used for simulation and prediction of ENSO (e.g., Zebiak and Cane, 1987; Zhang et al., 2003; Zheng et al., 2007; see the summary of model ENSO forecasts at the International Research Institute for Climate and Society (IRI) website: http://iri.columbia.edu/climate/ENSO/currentinfo/update.html). In CGCMs, FWF forcing is indeed included, but it has not been realistically represented. In particular, the so-called double ITCZ (intertropical convergence zone) problem remains challenging to CGCM simulations in the tropical Pacific.

Here, we continue to investigate the effects of FWF forcing using remote sensing data and an improved coupled ocean-atmosphere model with ocean biology-induced feedback also explicitly taken into account (Zhang et al., 2009). New results emerge in our HCM simulations when these feedbacks are considered in a coherent way; some results are presented briefly below.

2. Data and models

Some satellite-based data are used for FWF-related feedback analyses and modeling studies. Monthly precipitation (P) data were acquired from the Global Precipitation and Climatology Project (GPCP; Adler et al., 2003); monthly evaporation (E) data were obtained from the Objectively Analyzed Air-Sea Fluxes (OAFlux; Yu and Weller, 2007). The P and E data for the period 1979–2008 were used to derive freshwater flux (FWF) fields, defined as P minus E ($P - E$; this value is positive when there is a flux from the atmosphere to the ocean). In addition, recent studies have demonstrated that ocean biology (OB) in the tropical Pacific can potentially affect the climate through the penetration depth of sunlight in the upper ocean (H_{p}), a primary parameter in coupling biology to physics. Here, ocean color data (McClain et al., 1998) were used to estimate ocean biology-related H_{p} fields to represent the bio-climate feedbacks in the coupled ocean-atmosphere system of the tropical Pacific (Zhang et al., 2009, 2011).

2.1 *A hybrid coupled model* (*HCM*)

A hybrid coupled model (HCM) was used to demonstrate the modulating effects on ENSO that can be induced by FWF and salinity variability in the tropical Pacific. The HCM consists of an ocean general circulation model (OGCM) and an empirical model for interannual wind stress anomalies, whose details can be found in Zhang et al. (2006, 2009), and Zhang and Busalacchi (2009). Figure 1 illustrates a schematic diagram for the HCM which explicitly takes into account the related feedback effects in the tropical Pacific climate system. In the hybrid coupled modeling context, the total wind stress forcing to the ocean can be separated into its climatological part (τ_{clim}) and interannually anomaly part (τ_{inter}), written as $\tau = \tau_{\mathrm{clim}} + \alpha_\tau \tau_{\mathrm{inter}}$. Similarly, the total FWF exchange between the atmosphere and ocean is sep-

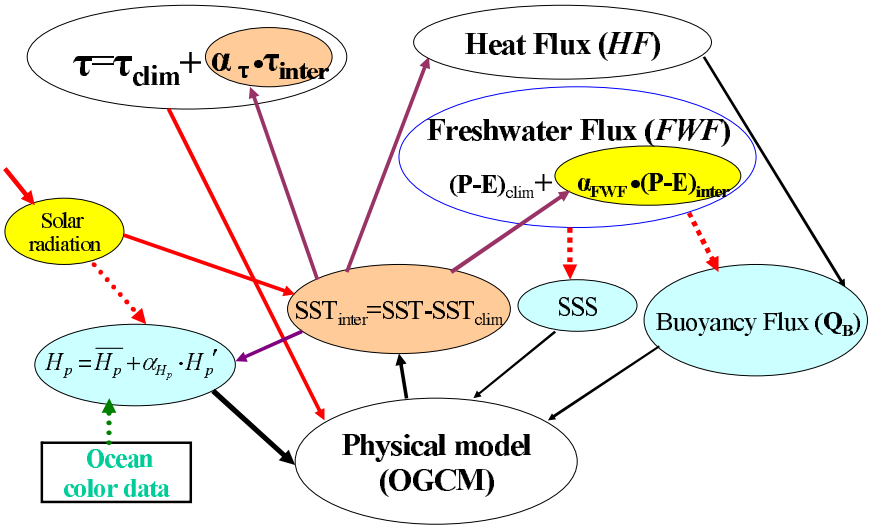

Fig. 1. A schematic diagram illustrating a hybrid coupled model (HCM) used to demonstrate the combined effects of freshwater flux (FWF) forcing and ocean biology (OB)-induced heating on the tropical Pacific ocean–atmosphere system. The HCM consists of an OGCM and a simplified atmospheric representation, whose three forcing fields to the ocean are included: wind stress (τ), freshwater flux (FWF), and heat flux (HF). The total wind stress (τ) is separated into its climatological ($\tau_{\rm clim}$) and interannual anomaly ($\tau_{\rm inter}$) parts: $\tau = \tau_{\rm clim} + \alpha_\tau \tau_{\rm inter}$. The total FWF, represented by precipitation minus evaporation, $(P-E)$, is also separated into its prescribed climatological $(P-E)_{\rm clim}$ and interannual anomaly [$\rm FWF_{inter}$ or $(P-E)_{\rm inter}$] parts: FWF $= (P-E)_{\rm clim} + \alpha_{\rm FWF}(P-E)_{\rm inter}$. These fields have direct effects on sea surface salinity (SSS) and buoyancy flux ($Q_{\rm B}$). The heat flux (HF) is calculated using an advective atmospheric mixed layer (AML) model. In addition, the climate system is affected by ocean biology in the region, whose effects on ocean physics are simply represented by the attenuation depth of solar radiation in the upper ocean ($H_{\rm p}$); similarly, the total $H_{\rm p}$ field is separated into its climatological part ($\overline{H_{\rm p}}$) and interannual anomaly part ($H'_{\rm p}$): $H_{\rm p} = \overline{H_{\rm p}} + \alpha_{H_{\rm p}} H'_{\rm p}$. Some scalar coefficients (α_τ, $\alpha_{\rm FWF}$, and $\alpha_{H_{\rm p}}$) are introduced to represent the strength of the corresponding feedbacks of interest. In this simplified coupled system, climatological fields [$\rm SST_{clim}$, $(P-E)_{\rm clim}$, and $\overline{H_{\rm p}}$] are prescribed to be seasonally varying; interannual anomaly fields [$\tau_{\rm inter}$, $\rm FWF_{inter}$ and $H'_{\rm p}$] are diagnostically determined from their corresponding empirical submodels, which are constructed using a singular value decomposition (SVD) analysis technique.

arated into its climatological part and interannually anomaly part: FWF $= (P-E)_{\rm clim} + \alpha_{\rm FWF}\,(PE)_{\rm inter}$; $H_{\rm p}$ is also written as $H_{\rm p} = \overline{H_{\rm p}} + \alpha_{H_{\rm p}} H'_{\rm p}$. Climatological parts ($\tau_{\rm clim}$, $(P-E)_{\rm clim}$, and $\overline{H_{\rm p}}$) are all prescribed using their long-term climatological fields (i.e., seasonally varying) from corresponding observations; interannual anomalies [$\tau_{\rm inter}$, $(P-E)_{\rm inter}$, and $H'_{\rm p}$] are calculated using empirical submodels derived from historical data. Some scalar parameters ($\alpha_\tau, \alpha_{\rm FWF}$, and $\alpha_{H_{\rm p}}$) are introduced to represent their feedback intensities. To represent the related feedbacks with a reasonable intensity, these scalar parameters were adopted as follows: $\alpha_\tau = 1.2$, $\alpha_{\rm FWF} = 1.0$, and $\alpha_{H_{\rm p}} = 2.0$ as explained in details by Zhang et al. (2006, 2009) and Zhang and Busalacchi (2009), respectively. Details of the interannual anomaly submodels for FWF and $H_{\rm p}$ are presented below.

2.2 *An empirical model for interannual FWF variability*

Interannual FWF anomalies in the tropical Pacific are dominated by ENSO signals, as demonstrated in Fig. 2b from the GPCP and OAFlux data. During El Niño, a warm SST anomaly causes an increase in P over the western-central tropical Pacific, with a positive FWF anomaly into the ocean. During La Niña, a cold SST anomaly is accompanied by a negative FWF anomaly (a net loss of freshwater from the ocean), which is primarily attributed to a deficit in P. Thus, there exists a coherent pattern between interannual variations in SST and FWF over the tropical Pacific, with a dominant SST control on FWF.

The satellite-based P and E data are used to construct an empirical parameterization for interannual FWF variability in the tropical Pacific (Zhang and

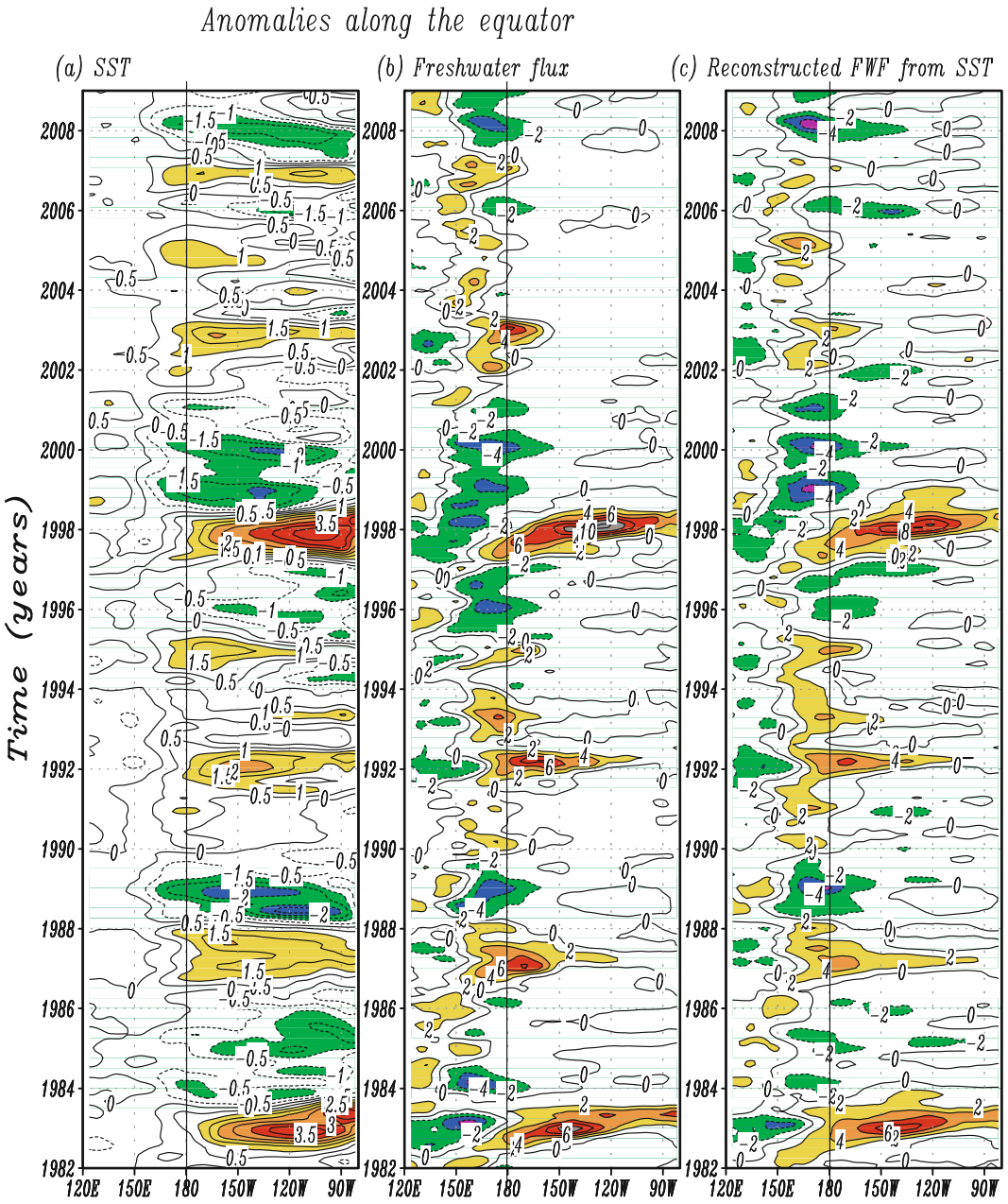

Fig. 2. Anomaly fields along the equator during 1982–2008: (a) observed SST from Extended Reconstructed Sea Surface Temperature (ERSST) data, (b) (P−E) from the GPCP and OAFlux data, and (c) (P−E) constructed using the SVD-based empirical model from the SST anomalies shown in (a). The contour interval is 0.5°C in (a), and 2 mm d^{-1} in (b) and (c).

Busalacchi, 2009). To determine statistically optimized empirical modes of interannual co-variabilities between FWF and SST, a singular value decomposition (SVD) technique is adopted. The SVD analysis is performed using historical SST and FWF anomaly fields during the period 1979–2008 (a total of 30 years). The seasonality is taken into account by constructing seasonally dependent models for interannual $(P-E)$ variability, written as $(P-E)_{\text{inter}}$: the SVD analyses are performed separately for each calendar month, and thus the $(P-E)_{\text{inter}}$ model consists of 12 different submodels, one for each calendar month (e.g., Zhang et al., 2006). From the consideration of the sequence of the singular values and the reconstruction testing of the FWF anomaly fields from SST anomalies, the first five leading SVD modes are retained for the empirical model to have reasonable amplitude in estimating $(P-E)_{\text{inter}}$ fields. Thus, given an SST anomaly, in-

terannual FWF variability associated with ENSO can be empirically determined in the tropical Pacific.

Figure 2c exhibits the FWF anomalies reconstructed using the empirical FWF model from the given SST anomalies (Fig. 2a). The model very well captures large-scale interannual $(P - E)$ variability associated with ENSO evolution. For example, the spatial pattern of large-scale FWF variability at the mature phase of El Niño or La Niña events can be depicted very realistically, with largest anomalies over the ITCZ in the central and eastern tropical Pacific. The amplitude of the reconstructed FWF anomalies (Fig. 2c) can be comparable to the original field (Fig. 2b), with the reconstructed variance >70% in the central and eastern tropics. Thus, most of the FWF variability can be captured by the SVD-based empirical model from interannual SST anomalies. However, the simulated FWF anomalies are somewhat weaker, smoothed, and less noisy.

2.3 *An empirical model for the penetration depth* (H_p) *related with ocean biology-induced heating*

Recent observational and modeling studies have demonstrated that ocean biology can potentially affect the climate in the tropical Pacific (e.g., Chavez, 1999; Murtugudde et al., 2002; Ballabrera-Poy et al., 2007). Following Murtugudde et al. (2002) and Ballabrera-Poy et al. (2007), the effect can be simply represented by H_p, a primary parameter in coupling biology to physics. Now, H_p can be derived using chlorophyll (Chl) content data that are available from ocean color imagery since 1997 (e.g., McClain et al., 1998). In this study, Chl concentration data from SeaWiFS during the period September 1997–April 2007 were used to characterize interannual H_p variability in the tropical Pacific and to quantify its relationships with physical fields. In particular, an empirical model for interannual H_p variability was derived from satellite ocean color data to represent a coupled bioclimate feedback in the tropical Pacific (Zhang et al., 2009, 2011). This statistical modeling approach allows diagnostic determination of interannual H_p variations from SST anomalies without explicitly involving a comprehensive marine ecosystem model. As such, the related ocean biology-induced heating effect on ENSO can be taken into account in the hybrid coupled ocean-atmosphere modeling system of the tropical Pacific (Zhang et al., 2006).

2.4 *Model experiments*

The OGCM was initiated from the World Ocean Atlas (WOA01) temperature and salinity fields, and was integrated for 20 years using atmospheric climatological forcing fields. A hybrid coupled ocean-atmosphere experiment was then started from this OGCM spinup run, with an imposed westerly wind anomaly for 8 months (Zhang et al., 2006). Thereafter, the evolution of the coupled system was determined solely by coupled ocean-atmosphere interactions in the tropical Pacific. The coupled model was integrated for 30 years; the end of this 30-year simulation was arbitrarily denoted as year 2024. As shown by Zhang et al. (2006), the model has the ability to depict interannual oscillations associated with ENSO.

To illustrate the effects of interannual FWF forcing, two HCM simulations were performed. A reference run was performed, denoted as $\mathrm{FWF}_{\_\mathrm{inter}}$, in which both interannual FWF and H_p anomalies were diagnostically determined using their respective empirical submodels for the HCM (Fig. 1). Another climatological FWF run was performed, denoted as $\mathrm{FWF}_{\_\mathrm{clim}}$, in which FWF was prescribed to have seasonally varying climatology [i.e., the $(P-E)_{\mathrm{inter}}$ field is not taken into account and thus the related interannually varying FWF feedback was excluded]. These two experiments were started from the end of the 30-year coupled simulation (year 2024) and continued to year 2070.

3. Impacts of interannual FWF variability on ENSO

Examples of simulated fields from the two runs are shown in Figs. 3–7. The HCM produced well the mean ocean climatology and its variability in the tropical Pacific. Climatological features in the region included the warm pool in the west and the cold tongue in the east (Fig. 3). Seasonally, large variations in SST occurred in the eastern equatorial Pacific: warming took place during the spring and cooling occurred during the fall. Fresh waters were located in the far western equatorial Pacific; saline waters were located in the central basin, with a front near the date line (Fig. 4). The mixed layer was deep in the west but shallow in the east (not shown).

Furthermore, the HCM simulations also quite realistically depicted interannual oscillations with a ∼4-year period (Fig. 5). As well known, interannual variability in the tropical Pacific is dominated by ENSO events, which are determined by the coupling among SST, winds and the thermocline (e.g., Bjerknes, 1969). In the results from our model, large longitudinal displacements were clearly evident of the warm/fresh pool in the west and the cold tongue in the eastern equatorial Pacific (Figs. 3–4). During El Niño, the cold tongue shrank in the east; warm waters in the west extended eastward along the equator, with the 26°C isotherm of SST moving east of 130°W. During La

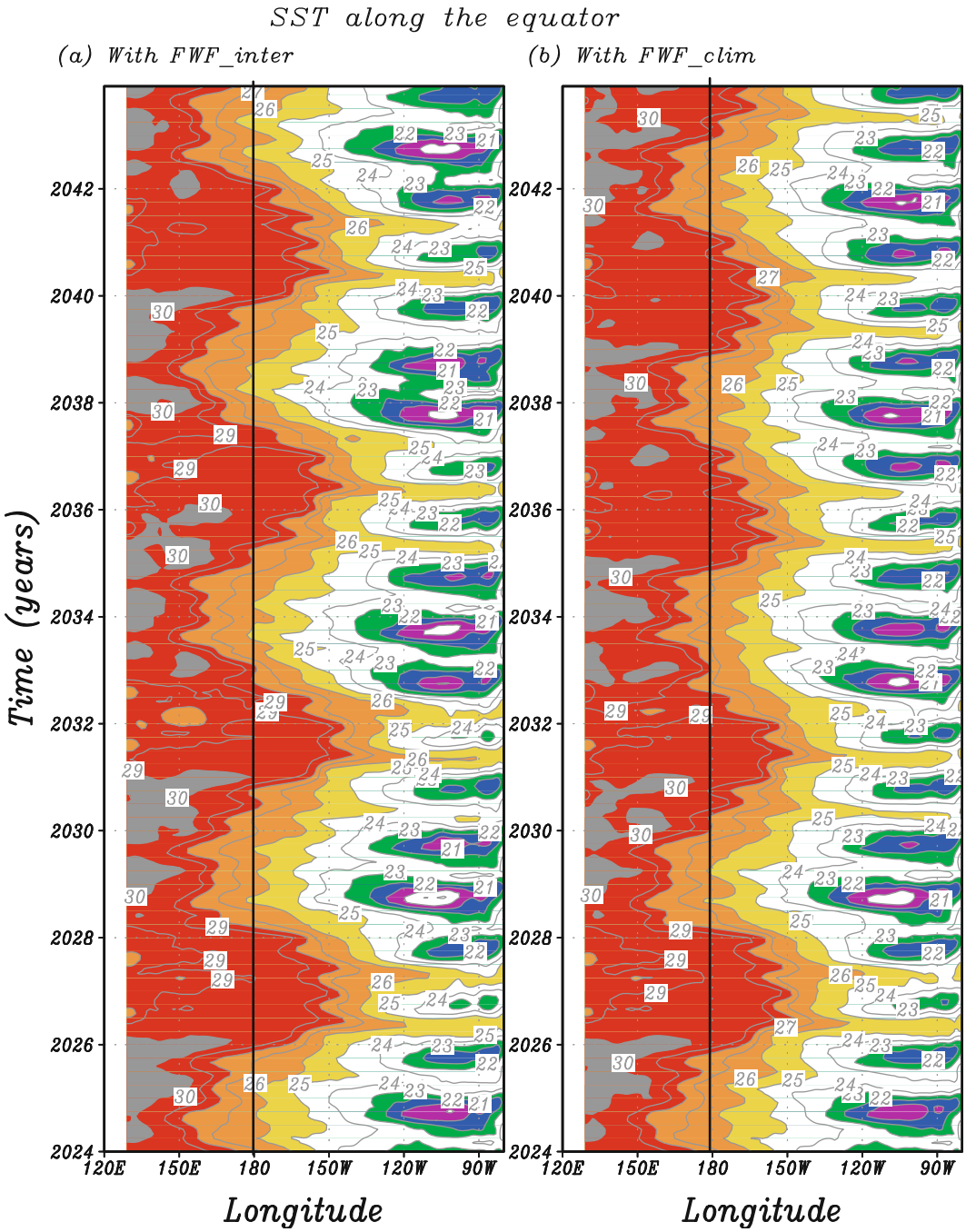

Fig. 3. The total SST fields along the equator simulated in the (a) $FWF_{\_inter}$ and (b) $FWF_{\_clim}$ runs. The contour interval is 0.5°C.

Niña, the warm pool retreated to the west; whereas the cold tongue developed anomalously strongly in the east and expanded westward along the equator, with the 25°C isotherm of SST moving west of 150°W. With these changes in SST, SSS had its largest variability around the eastern edge of the warm pool near the date line (Fig. 4). Associated with ENSO events, the SSS front near the date line also moved back and forth along the equator. During El Niño, a freshening occurred in the western and central basin, accompanied by its extension along the equator eastward beyond the date line. The interannual SSS variability was closely associated with FWF forcing which underwent large variations during ENSO cycles (Fig. 6a). These modeling simulations also show that the largest variability regions of SSS (Fig. 6b) were in the western-central basin, while those of SST were located in the central and eastern equatorial Pacific (Fig. 5a). The

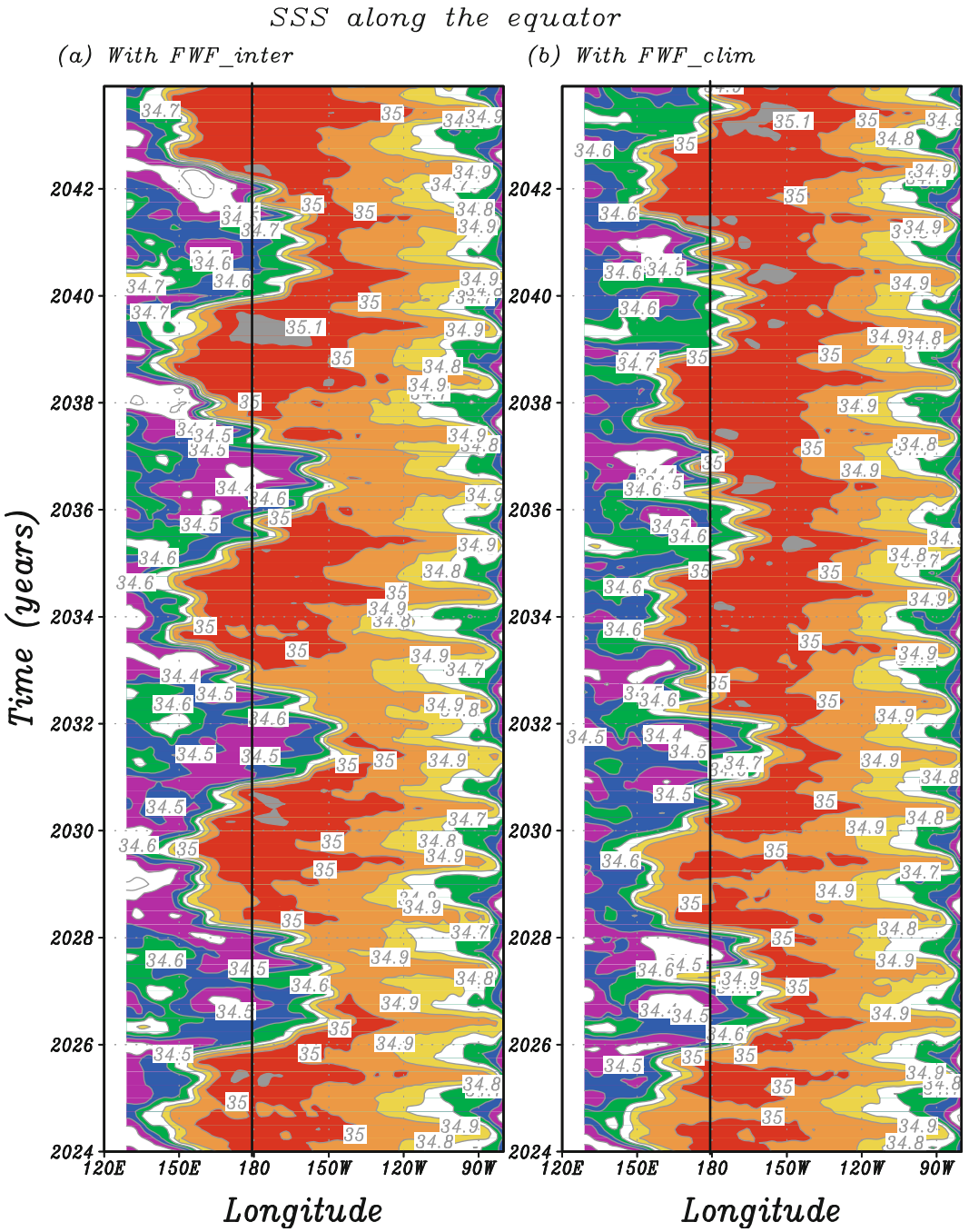

Fig. 4. The total SSS fields along the equator simulated in the (a) $FWF_{\_inter}$ and (b) $FWF_{\_clim}$ runs. The contour interval is 0.1 psu.

overall time scale of interannual variability simulated from this HCM, the spatio-temporal evolution, and the coherent phase relationships among various atmospheric and oceanic anomalies are consistent with observations, which have been extensively described (e.g., Zhang and Rothstein, 1998; Delcroix and Picaut, 1998).

Our comparison of these two runs also indicates that the FWF-induced climate feedback exerted a significant influence on interannual variability in the HCM simulations, which was evident in the $FWF_{\_inter}$ and $FWF_{\_clim}$ runs (Figs. 3–7). When the HCM started from the same initial condition, arbitrarily denoted as January 2024, the two HCM runs showed clear differences after several years of integration. For example, the SST evolution started to have notice-

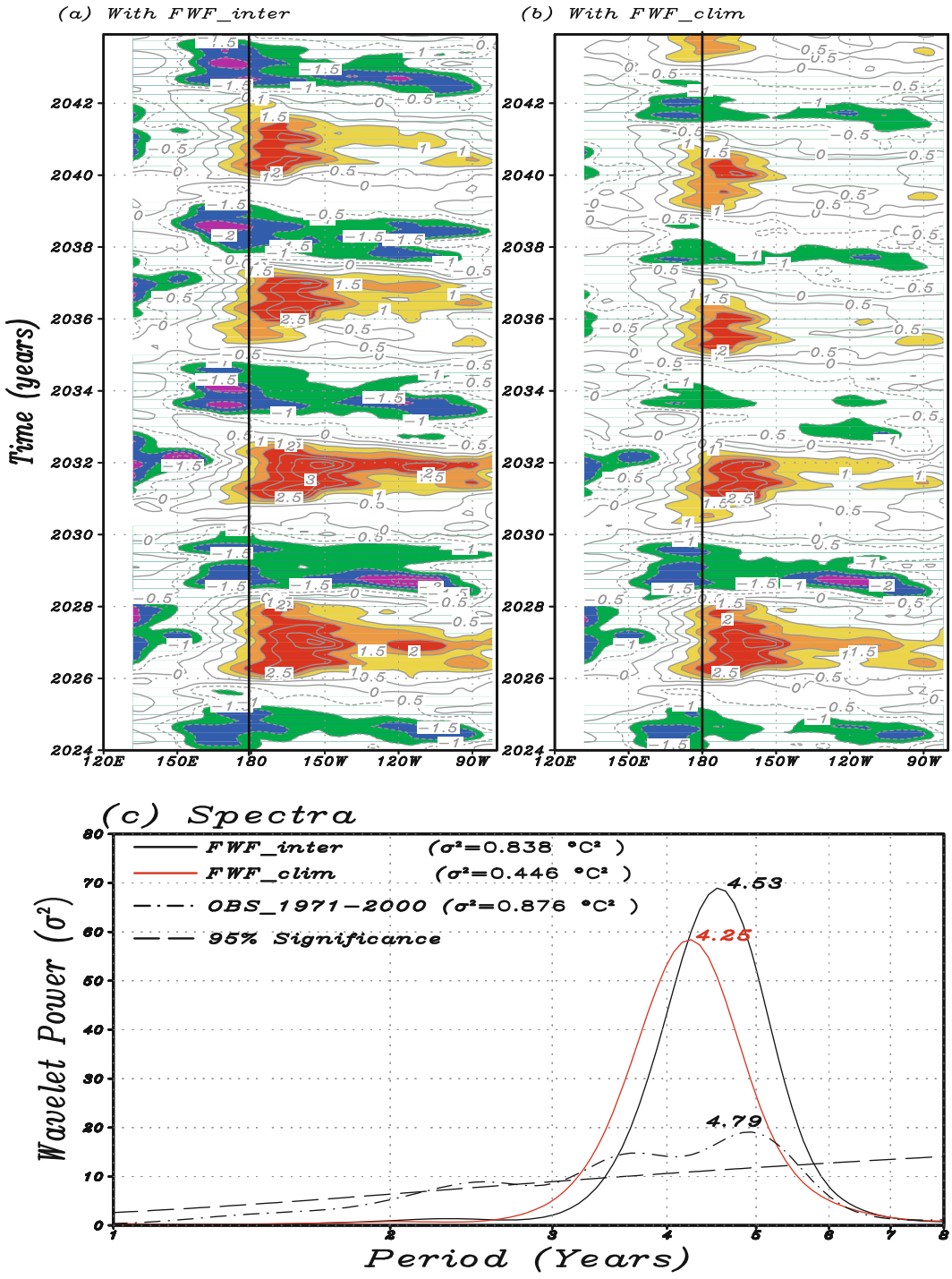

Fig. 5. Interannual SST anomalies along the equator simulated in the (a) $FWF_{\_inter}$ and (b) $FWF_{\_clim}$ runs, and (c) the corresponding wavelet power spectra for Niño3.4 SST anomalies. The observed estimate is based on the period 1971–2000 from the ERSST data. The dot-dashed line is the 95% confidence level for both runs, assuming a white noise process. The contour interval is 0.5°C in (a) and (b).

able differences in year 2032 and continues to show a systematic difference thereafter. In particular, a significant modulating effect emerged on ENSO amplitude and oscillation periods (e.g., Fig. 5). As evident in the comparisons from Figs. 3–7, interannual variability in the $FWF_{\_clim}$ run was substantially weaker; sometimes the amplitude of an individual ENSO event, represented by the Niño3.4 SST anomalies, caused a

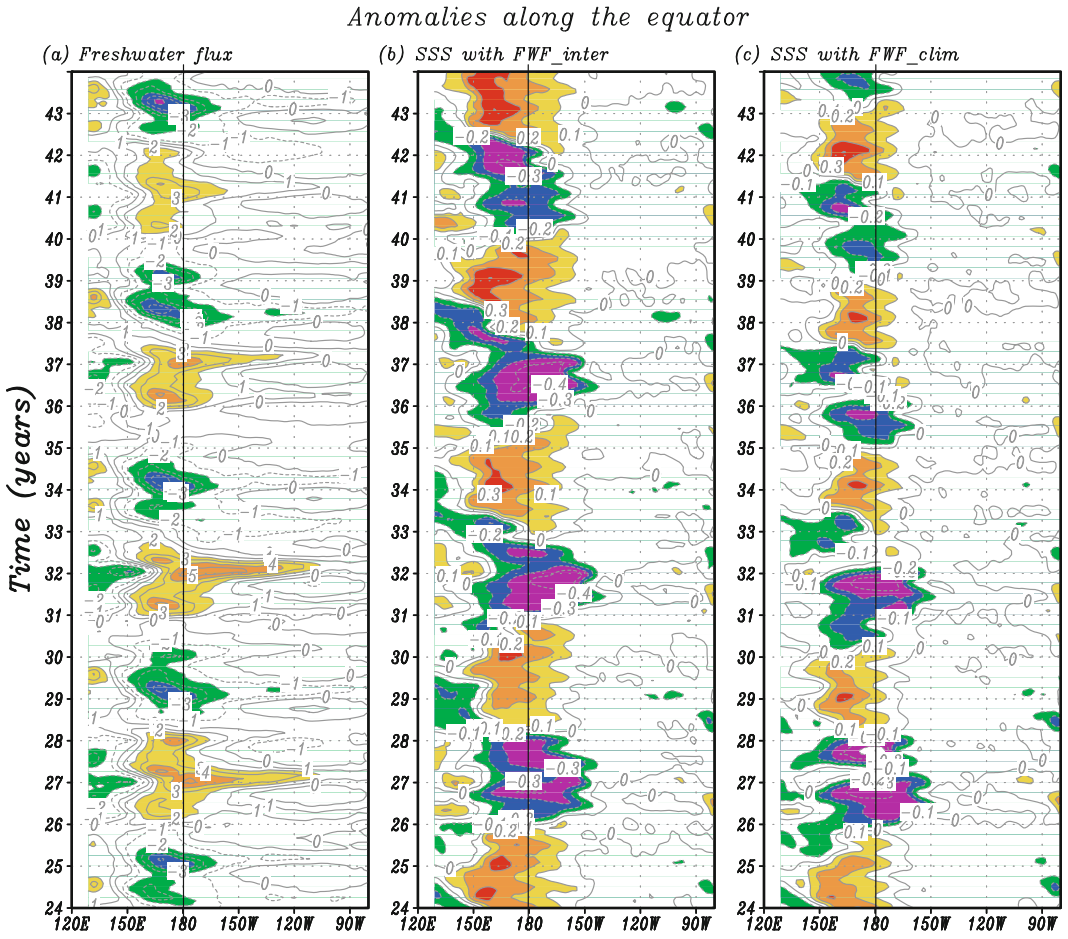

Fig. 6. Interannual variability along the equator: (a) FWF and (b) SSS simulated in the $FWF_{\_inter}$ run, and (c) SSS simulated in the $FWF_{\_clim}$ run. Note that the feedback induced by interannual FWF forcing is not included in the $FWF_{\_clim}$ run so that the SSS variability in this run is significantly weaker as compared with that in the $FWF_{\_inter}$ run. The contour interval is 1 mm d^{-1} in (a), and 0.1 psu in (b) and (c).

difference of >30% (e.g., in year 2032). Moreover, the two runs exhibited clear phase differences as well. For example, the ENSO time scale had a tendency to run shorter in $FWF_{\_clim}$ than in $FWF_{\_inter}$, indicating that the FWF-induced feedback effect caused a clear change in oscillation periods. The commonly used Niño indices at the Niño3.4 site were used to quantify the dominant time scales of interannual variability. As shown in Fig. 5c from a wavelet analysis, the interannual variability had a sharp peak at 4.5 years in the $FWF_{\_inter}$ run, but had a sharp peak at 4.3 years in the $FWF_{\_clim}$ run, with a difference of ∼4 months in oscillation periods. These results indicate that the FWF-induced feedback effects tend to modulate the ENSO time scales. Some of these effects were not seen in Zhang and Busalacchi (2009) and Zhang et al. (2009), where the two feedbacks induced by FWF and ocean biology were separately represented in these HCM modeling studies.

The effects were further quantified (Table 1). For

Table 1. The standard deviation of some selected anomaly fields in the $FWF_{\_inter}$ run and $FWF_{\_clim}$ run. Shown are for SST, zonal wind stress (τ_x) , and SSS at some selected Niño regions. The units are °C for SST, 10^{-5} N cm^{-2} for τ_x, and psu for SSS.

	SST				τ_x	SSS
	Niño4	Niño3.4	Niño3	Niño1.2	Niño4	Niño4
$FWF_{\_inter}$	0.96	0.97	0.84	0.58	0.21	0.19
$FWF_{\_clim}$	0.78	0.72	0.62	0.46	0.16	0.13

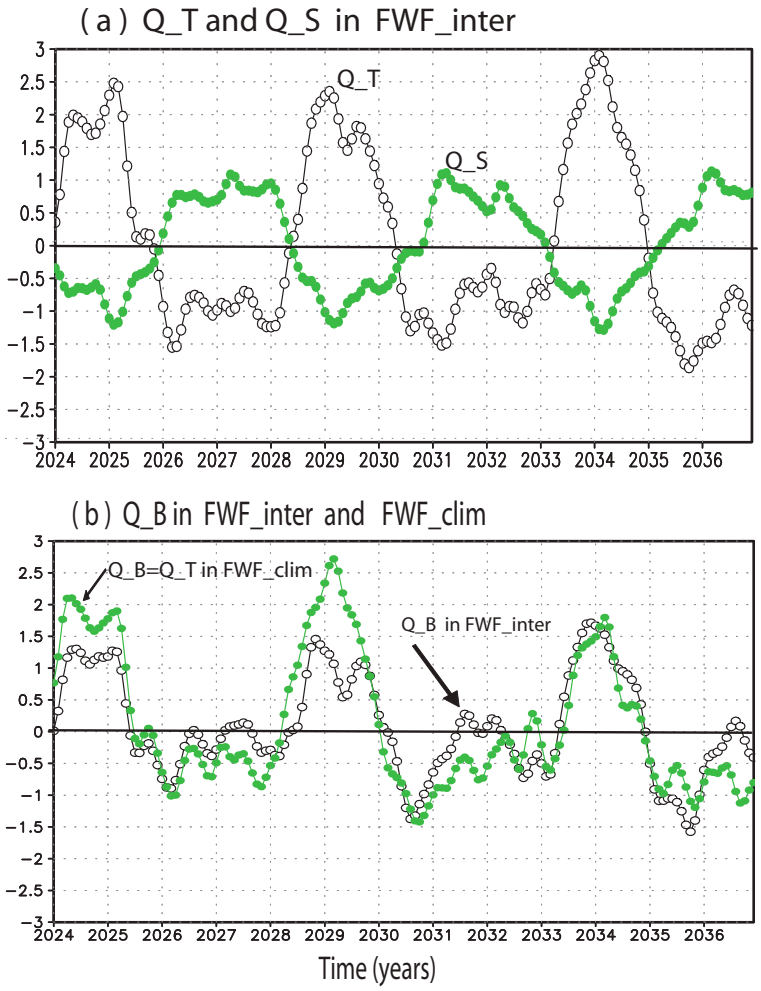

Fig. 7. Time series averaged in the region (5°S–5°N, 160°E–180°) for (a) the heat flux part (Q_T; line with open circles) and freshwater flux part (Q_S; line with solid circles) in the FWF_inter run, and for (b) the buoyancy flux (Q_B) in the FWF_inter run (line with open circles) and in the FWF_clim run (line with solid circles). The units in the figure are all expressed in 10^{-6} kg s^{-1} m^{-2}, which can be correspondingly converted to the commonly used units for heat flux and FWF (e.g., 1.0 $\times 10^{-6}$ kg s^{-1} m^{-2} is equivalent to 13.3 W m^{-2} for heat flux or to 3.4 mm d^{-1} for freshwater flux, respectively). Note that in the FWF_clim run in which interannual FWF forcing is not taken into account, $Q_S = 0.0$ and thus $Q_B = Q_T$. Also note that due to a compensating effect of interannual FWF forcing on Q_T, the resultant Q_B anomaly in the FWF_inter run is less negative during El Niño and less positive during La Niña (Fig. 7b), as compared with the FWF_clim run. As a result, the standard deviation of interannual Q_B variability calculated from these two HCM simulations during a 31-year period (from 2024 to 2054) is 1.22×10^{-6} kg s^{-1} m^{-2} in the FWF_inter run and 1.34×10^{-6} kg s^{-1} m^{-2} in the FWF_clim run, respectively.

example, the standard deviations of Niño3 and Niño4 SST anomalies were 0.62°C and 0.78°C, respectively, in the FWF_clim run; they were 0.84°C and 0.96°C, respectively, in the FWF_inter run. Relative to the FWF_clim run, these values represent an increase of ~19% and 24% for the Niño3 and Niño4 SST anomalies in the FWF_inter run, respectively. Also, the standard deviation of the Niño4 zonal wind stress was 0.16×10^{-5} N cm^{-2} in the FWF_clim run; it increased to 0.21×10^{-5} N cm^{-2} in the FWF_inter run (an increase by 31% in terms of wind stress variability). Also, the standard deviation of interannual SSS variability at the Niño4 site was 0.13 (1 psu=10^{-3}) in the FWF_clim run; it increased to 0.19 psu in the FWF_inter run, representing an increase of 46%. Thus, a significant fraction of the SST, surface wind, and SSS variability can be attributed to interannual FWF forcing effect. Note that in the FWF_inter run in which

$\alpha_{\rm FWF} = 1.0$ was taken to represent the FWF feedback, the simulated interannual FWF variability was substantially underestimated (Fig. 6a) compared with that estimated from observations (e.g., Fig. 2b). If the FWF-induced feedback intensity was increased to a reasonable level by using a larger $\alpha_{\rm FWF}$ (e.g., $\alpha_{\rm FWF} = 2.0$, cf. Zhang and Busalacchi, 2009), the resultant FWF-induced feedback effects on interannual variability in the HCM simulation would be expected to be stronger (as clearly demonstrated by Zhang and Busalacchi, 2009).

More analyses of phase relationships among interannual anomalies can be used to explain the interannual FWF forcing effect on the modulation of ENSO. It is well known that FWF exerts a direct influence on SSS and buoyancy flux ($Q_{\rm B}$) in the ocean. SSS is a state variable of the ocean that is controlled by the conservation equation of salt, an important variable to determine the oceanic density field, which in turn influences the upper ocean stability and vertical mixing. $Q_{\rm B}$ at the sea surface can be written as

$$Q_{\rm B} = \alpha {\rm HF}/(\rho c_p) + \beta S_0 {\rm FWF} = Q_{\rm T} + Q_{\rm S}$$

where HF is the net heat flux, FWF $= (P - E)$ is the net freshwater flux, α and β are the thermal and haline coefficients of expansion, S_0 is the reference surface salinity, c_p is the heat capacity, ρ is density of sea water. The convention used here is that positive buoyancy flux corresponds to an influx into the sea surface (a positive anomaly) so that the surface layer becomes more buoyant (or lighter) with reduced (upward) buoyant force. As expressed, $Q_{\rm B}$ at the sea surface results from a net contribution of the heat flux part ($Q_{\rm T}$) and freshwater flux part ($Q_{\rm S}$); this field serves as a direct forcing at the ocean-atmosphere interface that, together with wind, controls the evolution of MLD, which affects the entrainment of subsurface cold water into the mixed layer.

Figures 6 and 7 illustrate interannual variations in some related fields from the HCM simulations, including these flux components (i.e., $Q_{\rm S}$, $Q_{\rm T}$, and $Q_{\rm B}$). In the FWF$_{\rm _inter}$ run, these flux components exhibited coherent interannual variations during ENSO cycles. In the western-central tropical Pacific, FWF significantly contributed to $Q_{\rm B}$: the amplitude of interannual variability of $Q_{\rm S}$ was ~30% that of $Q_{\rm T}$ (Fig. 7a). Furthermore, interannual variations in $Q_{\rm S}$ were anticorrelated with those in $Q_{\rm T}$ during ENSO evolution (Fig. 7a). During El Niño, when warm SST anomalies were located in the central and eastern equatorial Pacific, a negative $Q_{\rm T}$ anomaly and a positive $Q_{\rm S}$ anomaly were seen in the western-central basin (Fig. 7a), with the latter ($Q_{\rm S}$) acting to reduce the amplitude of the former ($Q_{\rm T}$) directly. Due to the dominance of $Q_{\rm T}$ over $Q_{\rm S}$ in contributing to $Q_{\rm B}$, a negative $Q_{\rm B}$ anomaly was seen during El Niño (Fig. 7b; an anomalous loss of $Q_{\rm B}$ out of the ocean). Note that the direct offsetting effect of the positive $Q_{\rm S}$ anomaly on the negative $Q_{\rm T}$ anomaly made $Q_{\rm B}$ less negative during El Niño in the FWF$_{\rm _inter}$ run (Fig. 7b), which acted to decrease the MLD and reduce the entrainment of subsurface cold water into the mixed layer. During La Niña, cold SST anomalies were associated with a positive $Q_{\rm T}$ anomaly and a negative $Q_{\rm S}$ anomaly in the western-central basin (Fig. 7a). The resultant $Q_{\rm B}$ anomaly was positive (an anomalous gain of $Q_{\rm B}$ into the ocean). The offsetting effect of the negative $Q_{\rm S}$ anomaly on the positive $Q_{\rm T}$ anomaly led to the interannual $Q_{\rm B}$ anomaly that was less positive during La Niña in the FWF$_{\rm _inter}$ run (Fig. 7b), which acted to deepen the mixed layer and enhance the entrainment of subsurface cold water into the mixed layer. Thus, interannual FWF anomaly had a direct compensating effect on $Q_{\rm T}$ during ENSO cycles, causing reduced interannual $Q_{\rm B}$ variability, and modulation of the MLD and entrainment of subsurface cold water in the upper ocean.

Note that in the FWF$_{\rm _inter}$ run, the explicitly included interannual FWF forcing tended to induce stronger SST variability, which, in turn, caused larger interannual variability of heat flux ($Q_{\rm T}$ in Fig. 7a), as compared with the FWF$_{\rm _clim}$ run (Fig. 7b). As the amplitude of interannual $Q_{\rm T}$ variability increased, its contributing effects on $Q_{\rm B}$ increased as well, which should have led to an increase in interannual $Q_{\rm B}$ variability in the FWF$_{\rm _inter}$ run relative to the FWF$_{\rm _clim}$ run. However, as seen in Fig. 7b, this was not the case. Although interannual $Q_{\rm T}$ variability increased as a result of the FWF forcing effect on ENSO, the amplitude of interannual $Q_{\rm B}$ variability did not increase as with $Q_{\rm T}$; instead, the net contributions of $Q_{\rm S}$ and $Q_{\rm T}$ resulted in a reduction in interannual Q_B variability (Fig. 7b). Quantitatively estimated, the standard deviation of $Q_{\rm S}$ was 0.75 in the FWF$_{\rm _inter}$ run (the units for these values are all in 10^{-6} kg s^{-1} m^{-2}), whereas it was 0.0 in the FWF$_{\rm _clim}$ run (i.e., the interannual FWF forcing was not taken into account). The corresponding standard deviations of $Q_{\rm B}$ and $Q_{\rm T}$ were 1.22 and 1.64, resepectively, in the FWF$_{\rm _inter}$ run, and 1.34 and 1.34, respectively, in the FWF$_{\rm _clim}$ run.

These results can be utilized to illustrate a positive feedback between FWF and SST during ENSO cycles as follows (Fig. 8). ENSO cycles are characterized by SST anomalies over the equatorial regions, which induce a pronounced FWF response in the western and central basin, as represented by large interannual precipitation variability (Fig. 2). For example, during La Niña when SSTs are low in the eastern and central

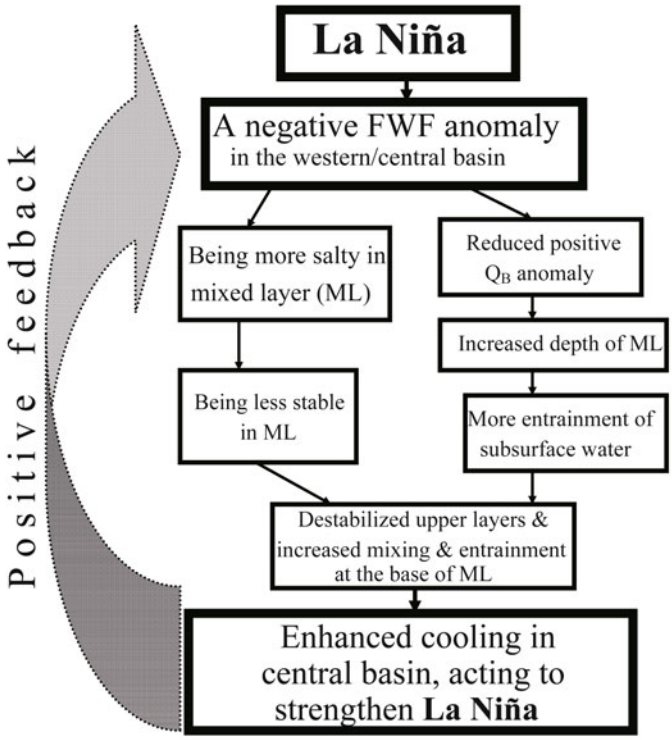

Fig. 8. A schematic diagram illustrating processes involved in the effects of a negative FWF anomaly induced by La Niña event.

tropical Pacific, a negative FWF anomaly is seen in the western and central basin (Fig. 6a). Its direct effects lead to salty surface waters; the induced changes in density (more dense in the mixed layer) act to weaken the stratification and thus destabilize the upper ocean, leading to increased vertical mixing at the base of the mixed layer. At the same time, the negative FWF anomaly makes the interannual Q_B anomaly less positive, which acts to deepen the mixed layer (ML) and enhance the entrainment of subsurface waters into the mixed layer. Through these direct effects of interannal FWF forcing on SSS and Q_B, the induced processes in the ocean tend to strengthen the vertical mixing and entrainment in the upper ocean. This acts to enhance the La Niña-related cold SST anomalies, with the Bjerknes feedback favoring further increase in upwelling and SST cooling. The effects of a positive FWF anomaly on El Niño can be also seen, but with the opposite effects. As a result, interannual FWF forcing tends to induce additional oceanic processes in the HCM that act to enhance the positive SST–wind–thermocline interactions, thus increasing the strength of interannual variability during ENSO cycles.

4. Concluding remarks

Understanding changes in the properties of ENSO remains a long-standing issue. Previous studies have focused on the role of wind and heat flux in the modulations of ENSO. As an important atmospheric forcing to the ocean, FWF has received increased attention in recent years due to its roles in ENSO processes and in support of satellite mission for remote sensing of precipitation and SSS (e.g., Lagerloef, 2002). In this study, we focused on the roles interannual FWF forcing plays in ENSO. Historical FWF data were utilized to develop an empirical model for representing FWF–induced climate feedback in the tropical Pacific. The derived FWF model was then incorporated into a basin-scale hybrid coupled ocean-atmosphere model in which ocean biology-induced feedback was also explicitly represented. Our results have demonstrated that FWF forcing can have significant effects on interannual variability, with positive feedback acting to enhance ENSO amplitude and lengthen its time scales. This mechanism can be explained as follows. During La Niña, a negative FWF anomaly leads to an increase in SSS and a reduced positive Q_B anomaly in the western-central basin. The former (through SSS) acts to increase the oceanic density fields, which destabilizes the upper ocean and enhances the vertical mixing; the latter (through Q_B) acts to increase the MLD, with more entrainment of cold subsurface water into the mixed layer. These related ocean processes act to strengthen the vertical mixing and entrainment in the upper ocean, which further enhance the cold SST

anomalies associated with the La Niña event. The effects of a positive FWF anomaly on El Niño can be seen similarly but with opposite effect. That is to say, the interannual FWF forcing-induced oceanic processes lead to more cooling during La Niña and more warming during El Niño in the tropical Pacific. This acts to enhance the positive SST–wind–thermocline interactions, with increased interannual variability and lengthened oscillation periods in the $\mathrm{FWF\_inter}$ run in which the interannual FWF forcing is taken into account.

These results support the view that the FWF-induced feedback and salinity variability can be a new contributor to ENSO variability. The large effects on ENSO demonstrated here indicate a clear need to adequately take into account this forcing in coupled ocean-atmosphere models. As FWF forcing has not been accurately included in most ICMs (e.g., Zheng et al., 2006, 2007, 2009; Zheng and Zhu, 2010) and HCMs (Zhang et al., 2006; Zhu et al., 2011) used for ENSO simulation and prediction, the empirical FWF model derived from satellite data in this work provides a simple way to parameterize the FWF feedback that can be easily incorporated into any coupled ocean–atmosphere model. Also, because this forcing significantly modulates ENSO, misrepresentations of FWF-induced feedback are a clear source of model biases in the tropical Pacific. Further modeling studies are underway to address these issues.

Acknowledgements. We would like to thank Tony Busalacchi, ZHU Jiang (IAP/CAS), Rui-Xin Huang (WHOI), WANG Dongxiao (SCSIO/CAS), and Dake Chen (SOED/SOA) for their comments. The authors wish to thank the two anonymous reviewers for their comments. This research is supported in part by NSF Grant (ATM-0727668 and AGS-1061998), NOAA Grant (NA08OAR4310885), and NASA Grants (NNX08AI74G, NNX08AI76G, and NNX09AF41G). F. Zheng is supported by the National Basic Research Program of China (Grant Nos. 2012CB417404 and 2012CB955202), and the Natural Science Foundation of China (Grant No. 41075064). Pei is additionally supported by China Scholarship Council (CSC) with the Ocean University of China, Qingdao, China.

REFERENCES

Adler, R. F., and Coauthors, 2003: The version-2 global precipitation and climatology project (GPCP) monthly precipitation analysis (1979–present). *Journal of Hydrometeorology*, **4**, 1147–1167.

Ballabrera-Poy, J., R. Murtugudde, R.-H. Zhang, and A. J. Busalacchi, 2007: Coupled ocean-atmosphere response to seasonal modulation of ocean color: Impact on interannual climate simulations in the tropical Pacific. *J. Climate*, **20**, 353–374.

Bjerknes, J., 1969: Atmospheric teleconnections from the equatorial Pacific. *Mon. Wea. Rev.,* **97**, 163–172.

Chavez, F. P., P. G. Strutton, G. E. Friedrich, R. A. Feely, G. C. Feldman, D. G. Foley, and M. J. McPhaden, 1999: Biological and chemical response of the equatorial Pacific ocean to the 1997–98 El Niño. *Science.* **286**, 2126–2131.

Collins, M., and Coauthors, 2010: The impact of global warming on the tropical Pacific Ocean and El Niño. *Nature Geoscience*, **3**, 391–397.

Delcroix, T., and J. Picaut, 1998: Zonal displacement of the western equatorial Pacific "fresh pool". *J. Geophys. Res.*, **103**, 1087– 1098.

Delcroix, T., S. Cravatte, and M. J. McPhaden, 2007: Decadal variations and trends in tropical Pacific sea surface salinity since 1970. *J. Geophys. Res.*, **112**, C03012, doi: 10.1029/2006JC003801.

Fedorov, A. V., R. C. Pacanowski, S. G. H. Philander, and G. Boccaletti, 2004: The effect of salinity on the wind-driven circulation and the thermal structure of the upper ocean. *J. Phys. Oceanogr.*, **34**, 1949–1966.

Hackert, E., J. Ballabrera-Poy, A. J. Busalacchi, R.-H. Zhang, and R. G. Murtugudde, 2011: Impact of sea surface salinity assimilation on coupled forecasts in the tropical Pacific. *J. Geophys. Res.,* **116**, C05009, doi: 10.1029/2010JC006708.

Huang, B., and V. M. Mehta, 2010: Influences of freshwater from major rivers on global ocean circulation and temperatures in the MIT ocean general circulation model. *Adv. Atmos. Sci.*, **27**, 455–468, doi: 10.1007/s00376-009-9022-6.

Lagerloef, G. S. E., 2002: Introduction to the special section: The role of surface salinity on upper ocean dynamics, air-sea interaction and climate. *J. Geophys. Res.*, **107**, 8000, doi: 10.1029/2002JC001669.

Maes, C., J. Picaut, and S. Belamari, 2002: Salinity barrier layer and onset of El Niño in a Pacific coupled model. *Geophys. Res. Lett.*, **29**(24), 2206, doi: 10.1029/2002GL016029.

McClain, C. R., M. L. Cleave , G. C. Feldman, W. W. Gregg, S. B. Hooker, and N. Kuring, 1998: Science quality SeaWiFS data for global biosphere research. *Sea Technology*, **39**, 10–16.

Murtugudde, R., and A. J. Busalacchi, 1998: Salinity effects in a tropical ocean model. *J. Geophys. Res.*, **103**, 3283–3300.

Murtugudde, R., J. Beauchamp, C. R. McClain, M. Lewis, and A. J. Busalacchi, 2002: Effects of penetrative radiation on the upper tropical ocean circulation. *J. Climate*, **15**, 470–486.

Timmermann, A., and F.-F. Jin, 2002: Phytoplankton influences on tropical climate. *Geophys. Res. Lett.*, **29**, 2104, doi: 10.1029/2002GL015434.

US CLIVAR Salinity Working Group, 2007: Report of the US CLIVAR Salinity Working Group. US CLIVAR Report No. 2007-1, US CLIVAR Office, Washington, D. C. [Available online at:

http://www.usclivar.org/Pubs/Salinity_final_report.pdf.]

Yang, S., K.-M. Lau, and P. S. Schopf, 1999: Sensitivity of the tropical Pacific ocean to precipitation-induced freshwater flux. *Climate Dyn.*, **15**, 737–750.

Yu, L., and R. A. Weller, 2007: Objectively analyzed air-sea heat fluxes for the global ice-free oceans (1981–2005). *Bull. Amer. Meteor. Soc.*, **88**, 527–539.

Yu, Y., W. Zheng, B. Wang, H. Liu, and J. Liu, 2011: Versions g1.0 and g1.1 of the LASG/IAP Flexible Global Ocean-Atmosphere-Land System Model. *Adv. Atmos. Sci.*, **28**, 99–117, doi: 10.1007/s00376-010-9112-5.

Zebiak, S. E., and M. A. Cane, 1987: A model El Niño/Southern Oscillation. *Mon. Wea. Rev.*, **115**, 2262–2278.

Zhang, R.-H., and L. M. Rothstein, 1998: On the phase propagation and relationship of interannual variability in the tropical Pacific climate system. *Climate Dyn.*, **14**, 713–723.

Zhang, R.-H., S. E. Zebiak, R. Kleeman, and N. Keenlyside, 2003: A new intermediate coupled model for El Nino simulation and prediction. *Geophys. Res. Lett.*, **30**, 2012, doi: 10.1029/2003GL018010.

Zhang, R.-H., A. J. Busalacchi, and R. G. Murtugudde, 2006: Improving SST anomaly simulations in a layer ocean model with an embedded entrainment temperature submodel. *J. Climate,* **19**, 4638–4663.

Zhang, R.-H., A. J. Busalacchi, and D. G. DeWitt , 2008: The roles of atmospheric stochastic forcing (SF) and oceanic entrainment temperature (T_e) in decadal modulation of ENSO. *J. Climate*, **21**, 674–704.

Zhang, R.-H., and A. J. Busalacchi, 2008: Rectified effects of tropical instability wave (TIW)-induced atmospheric wind feedback in the tropical Pacific. *Geophys. Res. Lett.,* **35**, L05608, doi: 10.1029/2007GL033028.

Zhang, R.-H., and A. J. Busalacchi, 2009: Freshwater flux (FWF)-induced oceanic feedback in a hybrid coupled model of the tropical Pacific. *J. Climate*, **22**(4), 853–879.

Zhang, R.-H., A. J. Busalacchi, X. Wang, J. Ballabrera-Poy, R. G. Murtugudde, E. C. Hackert, and D. Chen, 2009: Role of ocean biology-induced climate feedback in the modulation of El Niño-Southern Oscillation. *Geophys. Res. Lett.*, **36**, L03608, doi: 10.1029/2008GL036568.

Zhang, R.-H., D. Chen, and G. Wang, 2011: Using satellite ocean color data to derive an empirical model for the penetration depth of solar radiation (H_{p}) in the tropical Pacific Ocean, *J. Atmos. Oceanic Technol.,* **28**, 944–965, doi: 10.1175/2011JTECHO797.1.

Zheng, F., J. Zhu, R.-H. Zhang, and G.-Q. Zhou, 2006: Ensemble hindcasts of SST anomalies in the tropical Pacific using an intermediate coupled model. *Geophys. Res. Lett.*, **33**, L19604, doi: 10.1029/2006GL026994.

Zheng, F., J. Zhu, and R.-H. Zhang, 2007: Impact of altimetry data on ENSO ensemble initializations and predictions. *Geophys. Res. Lett.*, **34**, L13611, doi: 10.1029/2007GL030451.

Zheng, F., J. Zhu, H. Wang, and R.-H. Zhang, 2009: Ensemble hindcasts of ENSO events over the past 120 years using a large number of ensembles. *Adv. Atmos. Sci.*, **26**(2), 359–372, doi: 10.1007/s00376-009-0359-7.

Zheng, F., and J. Zhu, 2010: Coupled assimilation for an intermediated coupled ENSO prediction model. *Ocean Dyn.*, **60**, 1061–1073, doi: 10.1007/s10236-010-0307-1.

Zhu, J., Z. Sun, and G.-Q. Zhou, 2007: A note on the role of meridional wind stress anomalies and heat flux in ENSO simulations. *Adv. Atmos. Sci.*, **24**, 729–738, doi: 10.1007/s00376-007-0729-y.

Zhu, J., G. Zhou, R.-H. Zhang, and Z. Sun, 2011: On the role of oceanic entrainment temperature (T_e) in decadal changes of El Niño/Southern Oscillation. *Ann. Geophys.*, **29**, 529–540, doi: 10.5194/angeo-29-529-2011.